Bulk transport measurements in ZnO: The effect of surface electron layers

M. W. Allen,[1] C. H. Swartz,[1,*] T. H. Myers,[2,3] T. D. Veal,[4] C. F. McConville,[4] and S. M. Durbin[1]
[1]*The MacDiarmid Institute for Advanced Materials and Nanotechnology, University of Canterbury, Christchurch 8140, New Zealand*
[2]*Department of Physics, West Virginia University, Morgantown, West Virginia 26506, USA*
[3]*Materials Science and Engineering Program, Texas State University–San Marcos, San Marcos, Texas 78666, USA*
[4]*Department of Physics, University of Warwick, Coventry CV4 7AL, United Kingdom*
(Received 29 October 2009; revised manuscript received 8 January 2010; published 19 February 2010)

Magnetotransport measurements and x-ray photoemission spectroscopy were used to investigate the surface conductivity of ZnO. Near-surface downward band bending, consistent with electron accumulation, was found on the polar and nonpolar faces of bulk ZnO single crystals. A significant polarity effect was observed in that the downward band bending was consistently stronger on the Zn-polar face and weaker on the O-polar face. The surface electron accumulation layer was found to significantly influence the electrical properties of high resistivity, hydrothermally grown bulk ZnO crystals at temperatures below 200 K, and is largely responsible for the anomalously low electron mobility reported for this material.

DOI: 10.1103/PhysRevB.81.075211 PACS number(s): 72.80.Ey, 61.72.uj, 73.25.+i, 73.20.−r

I. INTRODUCTION

Oxide semiconductors—ZnO in particular—are attracting attention for their potential use in a variety of applications including high efficiency, ultraviolet light emitting diodes, ultraviolet solid state lasers, and high temperature, high frequency power electronics. A major hurdle to the realization of ZnO-based devices is its well publicized asymmetric doping nature, which heavily favors the formation of *n*-type material.[1] Another potential issue lies in the unusual surface properties of ZnO. It is well known that ZnO has an electrically active surface whose conductivity varies with ambient conditions.[2,3] This active surface has been successfully employed in gas sensing[4] and photocatalytic applications,[5] but may result in unwanted conduction paths between the contacts of electrical devices.[6] The conductivity of the ZnO surface may also affect measurements of its bulk electrical properties, particularly in the case of lightly doped or heavily compensated material.[7–9] The ability to separate surface and bulk contributions to the overall conductivity of ZnO is particularly relevant to the ongoing search for *p*-type material, as surface effects may mask the true electrical properties of *p*-type dopants.[7]

A major advantage of ZnO is the availability of high quality, bulk single crystals grown using a variety of techniques. The room temperature (RT) carrier concentration (n) of bulk ZnO grown by the hydrothermal (HT) method ($\sim 10^{14}$ cm^{-3}) is typically three orders of magnitude lower than material grown using the pressurized-melt (PM) and seeded-chemical-vapor-transport (SCVT) techniques.[10–12] This unusually low carrier concentration, attributed to a high concentration of compensating Group I acceptors,[9] makes HT ZnO an excellent material for studying the electrical nature of the ZnO surface. Combining magnetotransport measurements with the analytical methods of quantitative mobility spectrum analysis (QMSA) and multiple carrier fitting (MCF) creates a powerful tool for separating the influences of surface and/or interfacial conducting layers from the bulk properties of a sample.[13–16] In addition, valence-band x-ray photoemission spectroscopy (XPS) can be used to quantify the band bending associated with charge rearrangement in the near-surface region of semiconductors and has previously been used to investigate surface electron accumulation layers found in InN, InAs, In_2O_3, and CdO.[17–19] In this present study, we use a combination of magnetotransport measurements and valence-band XPS to investigate the surface conduction of ZnO and its variation with crystal polarity.

II. EXPERIMENTAL DETAILS

A. Magnetotransport measurements

Hall effect samples ($6\times6\times0.5$ mm^3) were cut from double sided polished, *c*-axis HT ZnO wafers from Tokyo Denpa Co. Ltd. (Japan). Ohmic Ti/Al/Pt contacts were fabricated on each corner of the Zn-polar (0001) face by electron beam evaporation. Resistivity and Hall effect measurements were made, using the van der Pauw technique, from 50–300 K in a helium flow cryostat. At each temperature, the resistivity (ρ) and Hall coefficient (R_H) of the sample were determined at 22 logarithmically spaced values of magnetic field from 0 to 12 T using a 12 T Janis XVM 19SG system at West Virginia University. The samples were held for at least 10 h in dark conditions prior to these measurements to minimize persistent photoconductivity effects. During the magnetic field ramps, the temperature of the sample was held to within ±0.002 K to avoid distortion of the field dependency of ρ and R_H. At selected temperatures, the field was ramped in both the positive and negative directions which confirmed that any asymmetry in the measurements was negligible.

The measured values of $\rho(B)$ and $R_H(B)$ were converted to the *x*-*y* components of the conductivity tensor using

$$\sigma_{xx}(B) = \frac{\rho}{\rho^2 + (R_H B)^2} = \sum_{i=1}^{N} \frac{\sigma_{0_i}}{1 + (\mu_i B)^2} \tag{1}$$

and

$$\sigma_{xy}(B) = \frac{R_H B}{\rho^2 + (R_H B)^2} = \sum_{i=1}^{N} \frac{\sigma_{0_i} \mu_i B}{1 + (\mu_i B)^2}, \quad (2)$$

where B is the strength of the magnetic field applied in the z direction. All quantities are in SI units. Equations (1) and (2) also show how σ_{xx} and σ_{xy} can be expressed as the sum of separate contributions from multiple carrier populations of concentration n_i and mobility μ_i, where $\sigma_{0_i} = e n_i \mu_i$ is the conductivity of each population at zero magnetic field. As B increases, the paths of the higher mobility carriers are more heavily deflected and their contribution to σ_{xx} and σ_{xy} decreases. The dependences of σ_{xx} and σ_{xy} on B were simultaneously fitted using Eqs. (1) and (2) to extract n_i and μ_i for each resolvable carrier population. This was initially done using the QMSA algorithm which requires no *a priori* assumptions concerning the number of carriers[13–15] and which produces an almost continuous spectrum of the most likely distribution of carrier mobilities. QMSA was used to identify the number and type of discrete carrier populations which were used as input parameters for the more quantitatively accurate MCF procedure.[15] MCF assumes that the number of separate carrier species is known ($N=2$ in our case) and uses the Levenburg-Marquardt nonlinear least-squares fitting algorithm to determine the values of n_i and μ_i that provide the best fit to the experimentally determined σ_{xx} and σ_{xy} field dependencies.

B. Valence-band XPS

High resolution valence-band XPS measurements were performed at RT using a Scienta ESCA spectrometer at the National Centre for Electron Spectroscopy and Surface Analysis, Daresbury Laboratory, U.K. with the measurements repeated using a Kratos XSAM800 instrument at the University of Auckland, NZ. Both instruments were configured with a monochromatic rotating anode Al $K\alpha$ x-ray source ($h\nu = 1486.6$ eV) and a hemispherical electron energy analyzer with a multichannel detector providing an effective resolution of ~400 meV. Normal emission spectra were collected without the use of an electron flood gun from samples that were backside coated with indium and attached to a stainless steel sample holder using conducting tape. Provided samples are well-grounded to the instrument, the binding energy (BE) scale of the spectrometer can be referenced to the Fermi level of the sample. The BE scale of each instrument was calibrated using the Fermi edge of ion-bombarded silver and gold reference samples. The position of the valence-band maximum in the near-surface region of each sample was determined from a least-squares linear fit to the leading edge of the valence-band photoemission extrapolated to the instrument background. This accounts for the tail introduced in the valence-band spectrum by the finite resolution of the spectrometer.[26]

III. RESULTS AND DISCUSSION

A. Magnetotransport measurements

At each temperature QMSA indicated the presence of two distinct carrier populations: a high-mobility bulk electron

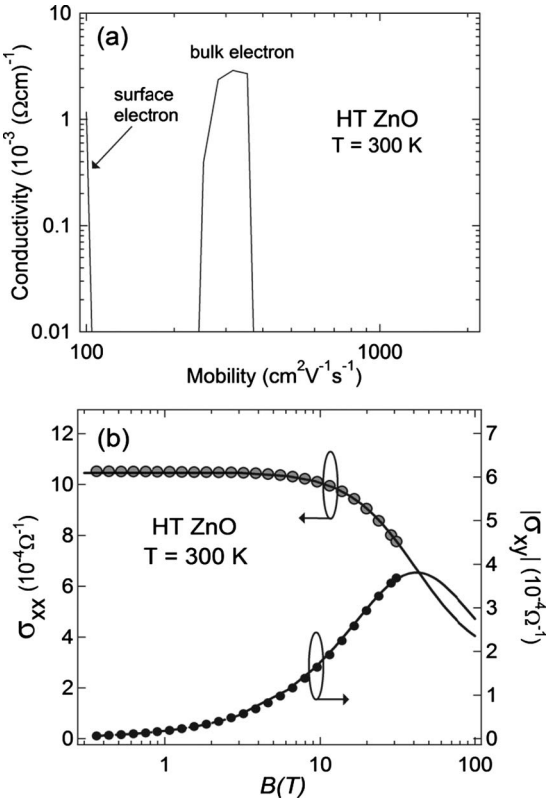

FIG. 1. (a) QMSA mobility spectrum and (b) sheet conductivity tensor components σ_{xx} and σ_{xy} for HT ZnO at 300 K, fitted using MCF analysis assuming $N=2$ electron populations, from magnetotransport measurements using van der Pauw contacts on the Zn-polar face.

($n_{\text{bulk}}, \mu_{\text{bulk}}$) and a significantly lower mobility surface electron ($n_{\text{surf}}, \mu_{\text{surf}}$). The low-mobility electron is assigned to the surface layer based on evidence from valence-band XPS measurements. It was not possible to resolve the mobility of the surface electron because it was below the resolution limit of $(\mu_i B)^2 > 0.01$. Subsequent measurements using a 35 T resistive magnet at the National High Magnetic Field Laboratory, Tallahassee, USA, were still unable to unambiguously resolve its mobility, although an upper limit of ~30 $cm^2\ V^{-1}\ s^{-1}$ at RT can be given. Figure 1 shows a typical QMSA mobility spectrum obtained at 300 K and the MCF of σ_{xx} and σ_{xy} assuming two discrete electron populations.

Due to the low mobility of the surface electron population, only the product $n_{\text{surf}}\mu_{\text{surf}}$ provides a significant contribution to Eqs. (1) and (2). Fortunately, MCF can be used to remove the effect of the low-mobility surface layer since the high-mobility bulk electron dominates the field dependence of σ_{xx} and σ_{xy} and therefore the fitting procedure converges to specific values for μ_{bulk} and n_{bulk}. Figure 2 shows the result of this process as a function of temperature. Values of n and μ obtained from single magnetic field Hall effect (SFH) measurements at 0.60 T that include the contribution of the surface layer, are shown for comparison. The temperature dependence of n_{bulk} is consistent with that of the donors—two closely lying deep defect levels at ~320 meV and several shallow impurity donors (such as Al, Fe, H) at

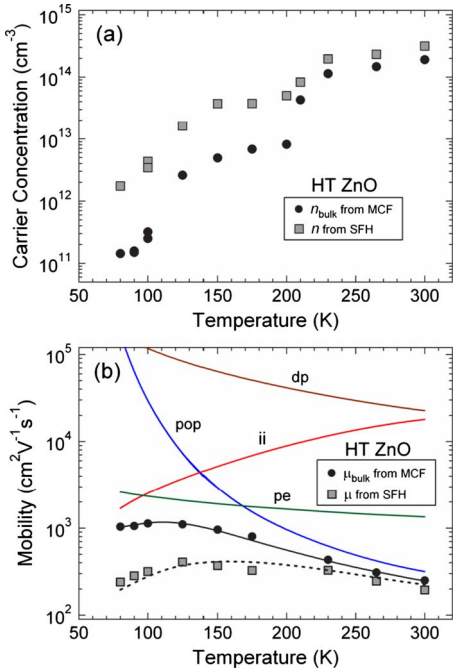

FIG. 2. (Color online) Temperature dependence of (a) the bulk carrier concentration (n_{bulk}: solid circles), and (b) the bulk electron mobility (μ_{bulk}: solid circles) of HT ZnO, from MCF analysis of magnetotransport measurements using van der Pauw contacts on the Zn-polar face. Single magnetic field Hall effect (SFH) measurements at 0.60 T (gray squares) which include the effect of the surface electron are shown for comparison. Figure 2(b) also shows a least-squares fit to the bulk electron mobility and the contributions from polar optical phonon scattering (pop), piezoelectric scattering (pe), deformation potential scattering (dp), and ionized impurity scattering (ii).

~13–52 meV—previously identified using thermal admittance and deep level transient spectroscopy in similar HT ZnO material from the same manufacturer.[20]

At RT, the effect of the surface layer on the overall conductivity of the sample is relatively minor. However, at temperatures below 200 K, the deep ~320 meV donors that control the RT conductivity of HT ZnO start to "freeze out" and the surface electron population now has a significant effect on both the carrier concentration [Fig. 2(a)] and the mobility [(Fig. 2(b)] of the sample. The maximum 'single field' mobility is 400 cm^2 V^{-1} s^{-1} at 125 K, which is consistent with the anomalously low maximum electron mobilities previously reported for HT ZnO using conventional (single magnetic field) Hall effect measurements.[9,21,22] Once the effect of the low-mobility surface electron is removed, the maximum bulk mobility rises to 1100 cm^2 V^{-1} s^{-1} at 110 K, which is comparable to the "single field" mobilities reported for PM and SCVT grown material.[22,23]

The temperature dependence of the bulk electron mobility was fitted, as shown in Fig. 2(b), using the common intrinsic scattering mechanisms [i.e., polar optical phonon scattering (pop), piezoelectric scattering (pe) and deformation potential scattering (dp)] combined with coulomb scattering from ionized impurities (ii). Well established expressions and parameters were used to determine the separate mobilities for each scattering mechanism which were then combined using Matthiessen's rule.[24,25] In particular, the Brooks-Herring model was used to describe ionized impurity scattering with the ionized impurity density as a fitting parameter. Significantly, an excellent fit to the bulk electron mobility of HT ZnO was achieved without the need to invoke additional scattering mechanisms.[22] A least-squares analysis yielded an ionized impurity density of 1.1×10^{16} cm^{-3}, an order of magnitude lower than the overestimated value of $\sim1\times10^{17}$ cm^{-3} that would be obtained from fitting the single field (0.60 T) data. Capacitance-voltage measurements on samples from the same wafer yielded a net donor density of 2×10^{15} cm^{-3}, confirming the highly compensated nature of HT ZnO.

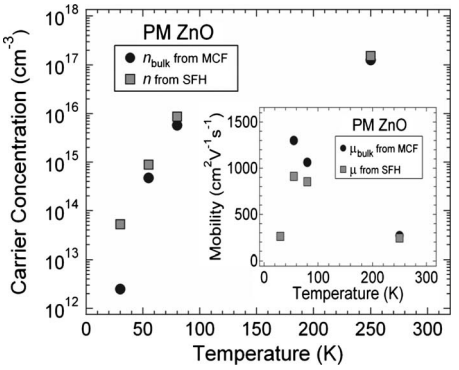

FIG. 3. Temperature dependence of the bulk carrier concentration (n_{bulk}: solid circles), and (inset) the bulk electron mobility (μ_{bulk}: solid circles), of PM ZnO from MCF analysis of magnetotransport measurements using van der Pauw contacts on the Zn-polar face. SFH measurements at 0.60 T (gray squares) are shown for comparison.

Although the surface can significantly affect the measured electrical properties of HT ZnO, this is not the case for uncompensated ZnO material. Figure 3 shows the results of MCF analysis of similar magnetotransport measurements on a c-axis PM ZnO wafer from Cermet Inc. (USA). Conventional van der Pauw contacts were again fabricated on the Zn-polar face. At RT, the bulk carrier concentration was three orders of magnitude higher than for HT ZnO. The electrical properties of PM ZnO are dominated by uncompensated shallow donors[22,23] and consequently the surface layer has a minor influence on the overall conductivity at temperatures above ~50 K.

For high resistivity HT ZnO, it is likely that the surface contribution to the magnetotransport measurements will be dominated by the crystal surface containing the van der Pauw contacts, especially at temperatures below 200 K. Similar magnetotransport measurements with identical contacts fabricated on the opposite O-polar $(000\bar{1})$ face also indicated the presence of a surface conduction layer. Interestingly, the conductance between any two ohmic contacts at 80 K appeared to be at least an order of magnitude lower for the O-polar face contacts, suggesting that the surface conductivity may be weaker on this face.

B. Valence-band XPS

The difference in the surface conduction layer on the Zn-polar and O-polar faces of HT ZnO was investigated using

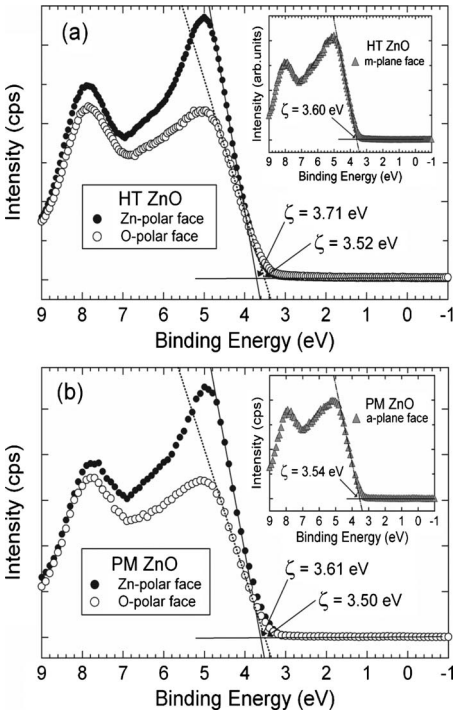

FIG. 4. Valence-band XPS spectra from the Zn-polar and O-polar faces of (a) the same bulk *c*-axis HT ZnO wafer and (b) the same bulk *c*-axis PM ZnO wafer showing the extraction of ζ, the valence-band maximum—Fermi level separation, for each face. The inset of Fig. 5(a) shows the spectrum from the m-plane face of a separate HT ZnO wafer. The inset of Fig. 5(b) shows the spectrum from the *a*-plane face of a separate PM ZnO wafer.

valence-band XPS. This is a useful tool for measuring the band bending in the near-surface region of a semiconductor. Figure 4(a) shows the valence-band XPS spectra collected from the Zn-polar and O-polar faces of the same *c*-axis HT ZnO wafer. The inset of Fig. 4(a) shows the spectrum collected from a separate *m*-plane $(1\bar{1}00)$ HT ZnO wafer $(n=3\times10^{14}\ \mathrm{cm}^{-3})$ from the same manufacturer. The energy difference $\zeta=E_V-E_F$ between the Fermi level (E_F) and the valence-band maximum (E_V) in the near-surface region of each face was determined by extrapolating a linear fit of the low BE edge of the valence-band spectrum to a line fitted to the instrument background.[26]

Table I gives the extracted values of ζ for each face. Since the RT band gap (E_g) of ZnO is 3.35 eV, the Fermi level at the Zn-polar, O-polar, and *m*-plane faces of HT ZnO lies in the conduction band. This indicates significant downward band bending and the presence of an electron accumulation layer at each face, consistent with the magnetotransport measurements. Table I also gives the magnitude of the downward band bending V_{bb}, calculated from $V_{bb}=E_g-\zeta-\xi$, where $\xi=(kT/q)\ln(N_C/n)$ is the energy difference between the Fermi level and the conduction band minimum in the bulk of the sample [N_C is the conduction band effective density of states $=2.94\times10^{18}\ \mathrm{cm}^{-3}$ for ZnO using $N_C=2(2\pi m_e^* kT/h^2)^{3/2}$ and an effective electron mass $m_e^*=0.24m_e$].

TABLE I. Values of ζ and V_{bb} measured using valence-band XPS on different crystal faces of HT and PM ZnO.

Material type and surface polarity	$\zeta=E_V-E_F$ (eV)	V_{bb} (eV)
HT Zn-polar	3.71 ± 0.02	−0.61
HT O-polar	3.52 ± 0.02	−0.42
HT *m*-plane	3.60 ± 0.02	−0.49
PM Zn-polar	3.61 ± 0.04	−0.34
PM O-polar	3.50 ± 0.04	−0.23
PM *a*-plane	3.54 ± 0.04	−0.29

The near-surface band bending and carrier concentration profiles at the Zn-polar and O-polar faces of HT ZnO were determined from a numerical solution of Poisson's equation within the modified Thomas-Fermi approximation (MTFA), with ζ and n_{bulk} as boundary conditions, as described elsewhere.[27] These are shown in Figs. 5(a)–5(d). The downward band bending is significantly (~190 meV) larger at the Zn-polar face of HT ZnO, indicating a stronger electron accumulation layer compared to the O-polar face. Figures 5(c) and 5(d) show a large increase in carrier concentration to $2.8\times10^{19}\ \mathrm{cm}^{-3}$ $[0.8\times10^{19}\ \mathrm{cm}^{-3}]$ at the Zn-polar [O-polar] face, which corresponds to a calculated surface sheet density of $7.1\times10^{12}\ \mathrm{cm}^{-2}$ $[2.8\times10^{12}\ \mathrm{cm}^{-2}]$.

Figure 4(b) shows the valence-band XPS spectra collected from the Zn-polar and O-polar faces of the same *c*-axis PM ZnO wafer $(n=1.5\times10^{17}\ \mathrm{cm}^{-3})$ from Cermet Inc. (USA). The inset of Fig. 4(b) shows the spectrum collected from a separate a-plane $(11\bar{2}0)$ PM ZnO wafer $(n=5\times10^{16}\ \mathrm{cm}^{-3})$ from the same manufacturer. The near-surface downward band bending (also given in Table I) for this material is significantly less than for HT ZnO, although the same V_{bb} trend with crystal polarity is observed. Figures 5(e)–5(h) show the calculated near-surface band bending and carrier concentration profiles at the Zn-polar and O-polar faces of PM ZnO. The corresponding surface sheet density $4.7\times10^{12}\ \mathrm{cm}^{-2}$ $[2.5\times10^{12}\ \mathrm{cm}^{-2}]$ at the Zn-polar [O-polar] face and the associated downward band bending is contained within a much narrower negative space charge region due to the much higher bulk carrier concentration of PM ZnO.

C. Surface Kelvin probe microscopy

Variations in the strength of the electron accumulation layer at different ZnO surfaces should also affect the surface dipole contribution to the work function of ZnO. Surface Kelvin probe microscopy was used to investigate the difference in the work function of the Zn-polar and O-polar faces of a number of similar HT ZnO wafers. These measurements were made at RT using a Digital Instruments 3100 Atomic Force Microscope and a gold coated cantilever tip in a low humidity environment, in dark conditions, with the samples exposed to air. The mean work function was 4.52 ± 0.03 $[4.70\pm0.03]$ eV on the Zn-polar [O-polar] surfaces with little lateral variation. The errors include both sample-to-sample and lateral variations. The lower work function on the Zn-polar face is consistent with the presence of a stronger

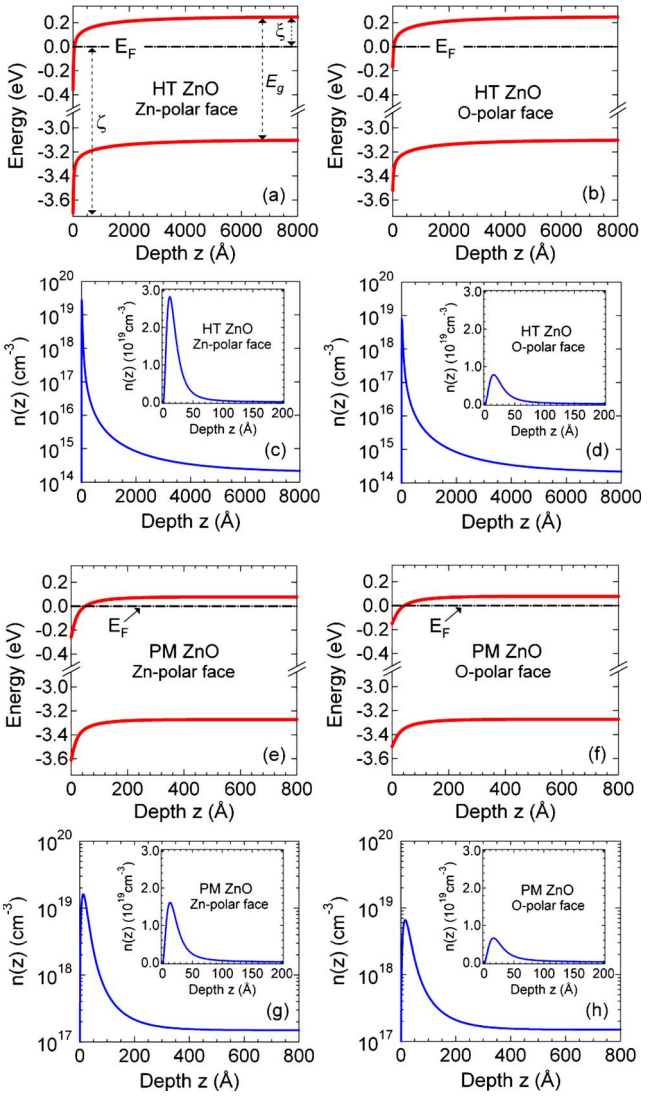

FIG. 5. (Color online) Poisson–MTFA calculations of the band banding and the carrier concentration profiles in the electron accumulation layer at the Zn-polar [(a) and (c)] and O-polar faces [(b) and (d)] of HT ZnO; and at the Zn-polar face [(e) and (g)] and O-polar face [(f) and (h)] of PM ZnO. (Input parameters were T=300 K, m_e^*=0.24m_e, ε_s=8.15, and E_g=3.35 eV).

electron accumulation layer (and a larger V_{bb}) compared to the O-polar face. These work function values lie between those published by Moormann *et al.*[28] using the vibrating gold wire (Kelvin) method on the Zn-polar (4.25 eV) and O-polar (4.95 eV) faces of ultra high vacuum cleaved, hexagonal vapor-phase grown ZnO crystals. The same authors reported a value of 4.64 eV for the m-plane face.

IV. DISCUSSION

To satisfy overall charge neutrality, the negative charge contained within the electron accumulation layer at the ZnO surface must screen an equal amount of fixed positive charge associated with unoccupied donor states, located at or very close to the surface. The identity of these surface donors is the subject of ongoing debate; possible candidates include extrinsic impurities, native defects, and surface hydroxide contamination.[29–31] It has been shown that the density of extrinsic donors (such as Al, Ga, In) and native donor defects can increase significantly near the ZnO surface.[29,30] XPS O 1*s* core level measurements consistently show the ZnO surface to be terminated with a persistent hydroxyl coverage.[31,32] It has also been proposed that H atoms donate approximately 0.5 electrons to each surface oxygen ion on both the OH terminated Zn-polar and O-polar ZnO surfaces and are the possible source of a shallow electron donor state.[31,33]

Surface electron accumulation layers have been observed in a number of other semiconductors including InN, InAs, In_2O_3, and CdO.[17–19] For each of these, the branch point energy (BPE) of the virtual gap states (ViGS) created when the periodicity of the crystal lattice is broken at surfaces and interfaces lies in the first conduction band.[34] This is a consequence of the large cation-anion size and electronegativity differences in these materials. Within the ViGS model, this unusual BPE position heavily favors the formation of near-surface donors which can donate their electrons directly into the conduction band, resulting in the formation of a surface accumulation layer. Schleife *et al.* recently calculated a BPE for ZnO of ~0.25 eV above the conduction band minimum,[34] providing a theoretical explanation for the *n*-type surface conductivity of ZnO in terms of its bulk band structure.

V. CONCLUSION

In summary, magnetotransport measurements were used to separate the effect of low-mobility surface electrons from the bulk electrical properties of ZnO. These surface electrons were found to have a significant influence on the electrical properties of high resistivity HT ZnO at temperatures below 200 K, and are a major cause of the anomalously low maximum electron mobility measured using single magnetic field Hall effect measurements. For PM ZnO, the surface layer has little effect on its electrical properties above 50 K due to the higher concentration of uncompensated shallow donors in this material. Valence-band XPS was used to quantify the near-surface band bending on the Zn-polar, O-polar, and *m*-plane faces of HT ZnO and on the Zn-polar, O-polar, and *a*-plane faces of PM ZnO. Downward band bending, consistent with electron accumulation, was measured on all these faces. A significant polarity effect was observed in HT ZnO [PM ZnO] in that the downward band bending on the Zn-polar face was 190 meV [110 meV] stronger compared to the O-polar face. Surface electron accumulation appears to be the natural state of both polar and nonpolar ZnO surfaces and can significantly influence electrical measurements made on heavily compensated ZnO material. Consequently it must be taken into account when investigating the electrical properties of potential *p*-type material.

ACKNOWLEDGMENTS

This work was supported by the Marsden Fund under Grant No. UOC0604. The assistance of G. Turner, C. Doyle,

and J. B. Metson is gratefully acknowledged. The facilities at West Virginia University were supported by an Office of Naval Research grant (Grant No. N00014-02-1-0974) and by the WVNano Initiative. The work at the National High Magnetic Field Laboratory was supported by NSF Cooperative Agreement under Grant No. DMR-0084173, the State of Florida, and the DOE. The work at the University of Warwick was supported by the EPSRC (Grant No. EP/G004447/1).

*Present address: Department of Physics, University of Southern Mississippi, Hattiesburg, MS 39402.

[1] S. B. Zhang, S. H. Wei, and A. Zunger, Phys. Rev. B **63**, 075205 (2001).
[2] G. Heiland and P. Kunstman, Surf. Sci. **13**, 72 (1969).
[3] M. Nakagawa and H. Mitsudo, Surf. Sci. **175**, 157 (1986).
[4] Q. Wan, Q. H. Li, Y. J. Chen, T. H. Wang, X. L. He, J. P. Li, and C. L. Lin, Appl. Phys. Lett. **84**, 3654 (2004).
[5] E. S. Jang, J.-H. Won, S.-J. Hwang, and J.-H. Choy, Adv. Mater. (Weinheim, Ger.) **18**, 3309 (2006).
[6] M. W. Allen, X. Weng, J. M. Redwing, K. Sarpatwari, S. E. Mohney, H. von Wenckstern, M. Grundmann, and S. M. Durbin, IEEE Trans. Electron Devices **56**, 2160 (2009).
[7] O. Schmidt, P. Kiesel, D. Ehrentraut, T. Fukuda, and N. M. Johnson, Appl. Phys. A: Mater. Sci. Process. **88**, 71 (2007).
[8] D. C. Look, H. L. Mosbacker, Y. M. Strzhemechny, and L. J. Brillson, Superlattices Microstruct. **38**, 406 (2005).
[9] D. C. Look, Superlattices Microstruct. **42**, 284 (2007).
[10] K. Maeda, M. Sato, I. Niikura, and T. Fukuda, Semicond. Sci. Technol. **20**, S49 (2005).
[11] J. Nause and B. Nemeth, Semicond. Sci. Technol. **20**, S45 (2005).
[12] D. C. Look, D. C. Reynolds, J. R. Sizelove, R. L. Jones, C. W. Litton, G. Cantwell, and W. C. Harsch, Solid State Commun. **105**, 399 (1998).
[13] W. A. Beck and J. R. Anderson, J. Appl. Phys. **62**, 541 (1987).
[14] J. R. Meyer, C. A. Hoffman, F. J. Bartoli, D. A. Arnold, S. Sivananthan, and J. P. Faurie, Semicond. Sci. Technol. **8**, 805 (1993).
[15] J. Antoszewski and L. Faraone, J. Appl. Phys. **80**, 3881 (1996).
[16] C. H. Swartz, R. P. Tompkins, N. C. Giles, T. H. Myers, H. Lu, W. J. Schaff, and L. F. Eastman, J. Cryst. Growth **269**, 29 (2004).
[17] T. D. Veal, P. H. Jefferson, L. F. J. Piper, C. F. McConville, T. B. Joyce, P. R. Chalker, L. Considine, H. Lu, and W. J. Schaff, Appl. Phys. Lett. **89**, 202110 (2006).
[18] P. D. C. King, T. D. Veal, P. H. Jefferson, J. Zúñiga-Pérez, V. Muñoz-Sanjosé, and C. F. McConville, Phys. Rev. B **79**, 035203 (2009).
[19] P. D. C. King, T. D. Veal, D. J. Payne, A. Bourlange, R. G. Egdell, and C. F. McConville, Phys. Rev. Lett. **101**, 116808 (2008).
[20] H. von Wenckstern, H. Schmidt, M. Grundmann, M. W. Allen, P. Miller, R. J. Reeves, and S. M. Durbin, Appl. Phys. Lett. **91**, 022913 (2007).
[21] R. Schifano, E. V. Monakhov, L. Vines, B. G. Svensson, W. Mtangi, and F. D. Auret, J. Appl. Phys. **106**, 043706 (2009).
[22] X. Yang and N. C. Giles, J. Appl. Phys. **105**, 063709 (2009).
[23] D. C. Look, Surf. Sci. **601**, 5315 (2007).
[24] D. C. Look, *Electrical Characterization of GaAs Materials and Devices* (Wiley, New York, 1990), Chap. 1.
[25] X. Yang, C. Xu, and N. C. Giles, J. Appl. Phys. **104**, 073727 (2008).
[26] S. A. Chambers, T. Droubay, T. C. Kaspar, and M. Gutowski, J. Vac. Sci. Technol. B **22**, 2205 (2004).
[27] P. D. C. King, T. D. Veal, and C. F. McConville, Phys. Rev. B **77**, 125305 (2008).
[28] H. Moormann, D. Kohl, and G. Heiland, Surf. Sci. **80**, 261 (1979).
[29] D. C. Look, B. Claflin, and H. E. Smith, Appl. Phys. Lett. **92**, 122108 (2008).
[30] B. J. Brillson, Y. Dong, D. Doutt, D. C. Look, and Z.-Q. Fang, Physica B **404**, 4768 (2009).
[31] B. J. Coppa, C. C. Fulton, P. J. Hartlieb, R. F. Davis, B. J. Rodriguez, B. J. Shields, and R. J. Nemanich, J. Appl. Phys. **95**, 5856 (2004).
[32] M. W. Allen, S. M. Durbin, and J. B. Metson, Appl. Phys. Lett. **91**, 053512 (2007).
[33] V. E. Henrich and P. A. Cox, *The Surface Science of Metal Oxides* (Cambridge University Press, Cambridge, England, 1994), p. 297.
[34] A. Schleife, F. Fuchs, C. Rödl, J. Furthmüller, and F. Bechstedt, Appl. Phys. Lett. **94**, 012104 (2009).